Biomimetic Remineralization of Carious Lesions by Self-Assembling Peptide

L. Kind[1], S. Stevanovic[1], S. Wuttig[1], S. Wimberger[1], J. Hofer[1], B. Müller[2], and U. Pieles[1]

Abstract

Caries is the most common disease in the world. Great efforts have been undertaken for prevention and to identify a regenerative treatment solution for dental caries. Self-assembling β-sheet forming peptides have previously shown to form 3-dimensional fiber networks supporting tissue regeneration. In particular, the self-assembling peptide P_{11}-4 has shown potential in the treatment and prevention of dental caries. It has previously been shown that application of monomeric P_{11}-4 solution to early carious lesions can increase net mineral gain by forming de novo hydroxyapatite crystals. The hypothesis for the mode of action was that monomeric self-assembling peptide P_{11}-4 diffuses into the subsurface lesion body and assembles therein into higher order fibrils, facilitating mineralization of the subsurface volume by mimicking the natural biomineralization of the tooth enamel, and it remains within the lesion body as a scaffold built-in by the newly formed hydroxyapatite. The aim of the present study was to investigate the mechanism of action of the self-assembling peptide P_{11}-4 supporting mineralization of carious enamel. By various analytical methods, it could be shown that the self-assembling peptide P_{11}-4 diffuses into the subsurface lesion, assembles into higher formed aggregates throughout the whole volume of the lesion, and supports nucleation of de novo hydroxyapatite nanocrystals and consequently results in increased mineral density within the subsurface carious lesion. The results showed that the application of self-assembling peptide P_{11}-4 can facilitate the subsurface regeneration of the enamel lesion by supporting de novo mineralization in a similar mode of action as has been shown for the natural formation of dental enamel.

Keywords: enamel biomineralization/formation, micro–computed tomography, regeneration, scanning electron microscopy (SEM), biomaterial(s), dentistry

Introduction

Caries

Caries is the most common disease worldwide (Petersen 2003; Kassebaum et al. 2015). It is caused by certain oral bacteria metabolizing carbohydrates into organic acids, consequently dissolving minerals making up enamel and dentin. Unlike dentine, enamel caries starts by subsurface demineralization, leaving a porous mineral surface covering the lesion body. After demineralization of approximately 30%, the mineralized surface collapses and breaks irreversibly (Bröchner et al. 2010; Bertassoni et al. 2011).

Demin/Remin Equilibrium

Within the oral cavity, there are alternating periods of demineralization caused by bacteria acids and remineralization facilitated by saliva (Hara and Zero 2010). During the demineralization process, calcium phosphate minerals, making up most of the enamel structure, is dissolved due to acidic pH and results in pores between crystallites. During remineralization, calcium phosphate supersaturated saliva redeposits minerals either on existing crystallites or triggers de novo formation of crystallites. This presents the natural regeneration process of the enamel tissue (ten Cate and Arends 1980).

Regeneration Approach

Present preventive approaches for caries, such as fluoride, mainly act by inhibiting demineralization by fluoride incorporation in the crystal lattice, resulting in lower solubility of the enamel (ten Cate 1997). The potential of fluoride to protect the enamel is restricted to the outer ~30 μm of the tooth (Schmidlin et al. 2016). A true regenerative approach, however, needs to aim at regenerating hydroxyapatite crystals within the subsurface

[1]School of Life Sciences, Department of Chemistry and Bioanalytics, University of Applied Sciences and Arts Northwestern Switzerland (FHNW), Muttenz, Switzerland
[2]Department of Biomedical Engineering, University of Basel, Biomaterials Science Center (BMC), Allschwil, Switzerland

Corresponding Author:
L. Kind, School of Life Sciences, Department of Chemistry and Bioanalytics, University of Applied Sciences and Arts Northwestern Switzerland (FHNW), Gründenstrasse 40, 4132 Muttenz, Switzerland.
Email: lucy.kind@fhnw.ch

carious lesion possibly using the natural remineralization process from saliva.

During odontogenesis, the enamel matrix enables formation of hydroxyapatite crystals to form enamel (Goldberg et al. 1995; Kirkham et al. 2000). However, the enamel matrix is mostly degraded during the final enamel maturation step and therefore is unavailable to support regeneration of larger defects during the tooth lifetime (Brookes et al. 2001). A biomimetic approach (i.e., mimicking the physiological function) would present the possibility to form de novo hydroxyapatite crystals (Hannig and Hannig 2010; Carneiro et al. 2016). Biocompatible small molecules capable of self-assembly diffusing into the subsurface carious lesion may be ideal building blocks for scaffolds guiding the regeneration of enamel tissue (Semino 2008; Li et al. 2011). Using peptide secondary structure motifs provided by amelogenin, itself a self-assembling molecular system, is one option investigated (Ruan and Moradian-Oldak 2015; Carneiro et al. 2016). Another is to use rationally designed small peptides that self-assemble into a 3-dimensional scaffold with surface characteristics mimicking the enamel matrix (Kirkham et al. 2007).

Self-Assembling Peptides

P_{11}-4 is a rationally designed small molecule that undergoes hierarchical self-assembly into fibrillar scaffolds in response to specific environmental triggers (Aggeli et al. 1997; Aggeli, Nyrkova, et al. 2001; Aggeli, Bell, Carrick, et al. 2003; Carrick et al. 2007). The peptide undergoes 1-dimensional self-assembly, forming micrometer-long nanotapes, ribbons, proceeding to the formation of fibrils, and edge-to-edge fibers (Nyrkova et al. 2000; Aggeli, Nyrkova, et al. 2001). This assembly process has been well characterized and is principally driven by intermolecular H-bonding arising from the peptide backbone, together with additional interactions between specific sidechains (Aggeli, Fytas, et al. 2001; Kayser et al. 2004). The design criteria for the peptides enabling the self-assembly are well understood and led to the development of a class of self-assembling peptides (Davies et al. 2009) with a number of candidates from the class showing potential in hard and soft tissue regeneration (Firth et al. 2006; Maude et al. 2013).

Self-Assembling Peptide P_{11}-4 as a Mimic for Enamel Matrix

As with any higher order molecular structure, the resulting surface of the 3-dimensional structure determines chemical and physical properties. P_{11}-4 assembled into fibers presents clusters of negative charges made up of 4 Glu-residues on its surface, presenting a potential Ca^{2+}-binding site. Molecular dynamics simulations have shown that those binding sites are approximately 9.4A apart—a distance found for the columnar Ca^{2+}-ions in the hydroxyapatite crystal (Thomson et al. 2014). Therefore, P_{11}-4 fibers present a suitable surface that could mimic the biological macromolecules found in mammalian

skeleton, where (predominantly anionic) matrix proteins are known to control the deposition and growth of hydroxyapatite crystals (Kirkham et al. 2002; Kirkham et al. 2007; Brunton et al. 2013).

P_{11}-4 Fibers to Support Remineralization

P_{11}-4 fibers have shown to support hydroxyapatite formation on its surface and the remineralization of early carious lesions in an in vitro pH-cycling model (Kirkham et al. 2007). In addition, in vitro remineralization tests have shown surface remineralization with formation of needle-shaped crystals (Takahashi et al. 2016), decrease of laser-fluorescence signal characteristic of early carious lesions (Jablonski-Momeni and Heinzel-Gutenbrunner 2014), and increased micro-hardness after remineralization of subsurface lesions (Schmidlin et al. 2016).

Furthermore, P_{11}-4 incorporated into a clinical product has shown encouraging results in early clinical trials improving the visual appearance of the carious lesions and showing increased opacity on X-rays after treatment of proximal caries (Brunton et al. 2013; Schlee et al. 2014).

This study investigates the proposed mechanism of action of the self-assembling peptide P_{11}-4 and the resulting fibers in promoting biomimetic regeneration or remineralization of early carious lesions. The following proposed mechanism of action is investigated in the present work: diffusion of monomers or small aggregates into the subsurface lesion, self-assembly into fibers or generally higher order aggregates within the carious lesion, and support of de novo crystallization of hydroxyapatite and resulting in remineralization of the lesion.

Materials and Methods

All chemicals, unless otherwise indicated, were purchased from Sigma-Aldrich. All buffer solutions were sterile filtered. Peptides were reconstituted in 20 mM Tris(hydroxymethyl)-aminomethan buffer (pH 8.4) resulting in a peptide concentration of 6.3 mM, but samples for Fourier transform infrared spectroscopy (FTIR) measurements were reconstituted in deuterium oxide (D_2O).

Creation of Artificial Carious Lesions in Human Enamel, Application of Self-Assembling Peptide P_{11}-4, and Remineralization Process

Creation of artificial lesions was performed as described by Lo et al. (2010): to define the position of the demineralized subsurface area (i.e., artificial carious lesion or white spot), the tooth was covered with colorless nail polish leaving a window of approximately 4 × 4 mm. The tooth was placed in demineralization buffer (2.2 mM $CaCl_2$, 2.2 mM NaH_2PO_4, 50 mM acetic acid; pH adjusted with 1 M KOH to 4.4) for 3 d at 37°C. The resulting subsurface lesions were pretreated with 10 µL of 2% NaClO (incubation for 1 min), rinsed, and air-dried at room temperature. Placebo-treated samples underwent identical pretreatment.

Table. Physical Properties of P_{11}-4 and its Variants Used in the Present Study.

Peptide	Sequence	Quality	Used Quantity by Experiment
P_{11}-4[a]	Ac-QQRFEWEFEQQ-NH$_2$	MW: 1,598 g/mol; lyophilized	6.3 mM (10 mg/mL)
^{14}C-P_{11}-4[b]	Ac[^{14}C]-QQRFEWEFEQQ-NH$_2$	MW: 1,599 g/mol, specific activity: 58 mCi/mmol (2.1 MBq/mmol); lyophilized	6.3 mM (10 mg/mL) (1:7; C-P_{11}-4: P_{11}-4)
ATTO647-P_{11}-4[c]	Ac-QQRFEWEFEQQSGSGC-(ATTO647)-NH$_2$	MW: 2,699.21 g/mol; lyophilized	6.3 mM (10 mg/mL) (1:20; ATTO647-P_{11}-4:P_{11}-4)
Placebo[a]	Bulking agent		6.3 mM (10 mg/mL)

Used peptide sequences were synthesized with solid-phase synthesis and purified by [a]CS Bio, [b]Hartmann Analytic GmbH, and [c]JPT Peptide Technologies GmbH. MW, molecular weight.

Application. In total, 10 µL (6.3 mM) peptide solution (P_{11}-4, P_{11}-4/^{14}C-P_{11}-4, P_{11}-4/ATTO647-P_{11}-4, or placebo [identical formulation without peptide]; Table) was applied, self-assembly was induced by 1 uL 35% H_3PO_4, incubated for 20 min, and placed in remineralization solution. Specimen samples with P_{11}-4 as well as the respective references were taken from the same tooth to avoid variability in results.

Remineralization. The samples were placed in remineralization buffer containing 2 mM $Ca(NO_3)_2$, 1.2 mM $KHPO_4$, and 60 mM Tris/HCl (pH adjusted to 7.4 with 1 M KOH) for 14 d by changing buffer every second day. A schematic drawing showing the proposed mechanism of action for regeneration of enamel using P_{11}-4 self-assembling peptides is presented in Figure 2 in Brunton et al. (2013).

Figure 1. Self-assembly of P_{11}-4. **(A)** Aggregation state of P_{11}-4 solution; A1: monomeric P_{11}-4 (6.3 mM) at pH >8, appearing as a liquid; A2: P_{11}-4 (6.3 mM) at pH 2, appearing as a nematic gel with high viscosity. **(B)** Nematic gel of P_{11}-4 under transmission electron microscopy (TEM) showing the network of fibers. **(C)** Higher magnification of nematic gel of P_{11}-4 under TEM showing individual fibers. The twist of the fibers can be detected. **(D)** FTIR spectrum from 1,700 to 1,580 cm^{-1}: P_{11}-4 (pH >8) as monomeric solution (black) with peak at 1,644 cm^{-1}, P_{11}-4 (pH 2) as a nematic gel (dark gray) with peak at 1,616 cm^{-1}, and placebo solution (light gray) without significant absorption in the region.

FTIR

A P_{11}-4 solution in D_2O was prepared. The sample was measured before and after acidification with deuterium chloride (DCl) using a Varian 670 FTIR Spectrometer with Golden Gate Diamond Attenuated Total Reflection (DATR) and a mercury-cadmium-telluride (MCT) detector (128 scans, resolution of 4 cm^{-1}).

Transmission electron microscopy reconstituted P_{11}-4 samples were diluted with water to a peptide concentration of 10.5 µM and applied to a carbon-coated copper grid (200 mesh). The grids were stained with uranyl acetate solution (2% w/v in water) for 40 s and washed twice with water. Examination was done with EM 900 (Zeiss) and a MegaView-III Camera (ESIS GmbH) at an accelerating voltage of 50 kV.

Congo Red Staining

After application of P_{11}-4 the enamel specimens were either washed in remineralization buffer for 1 h or without this washing step. The speci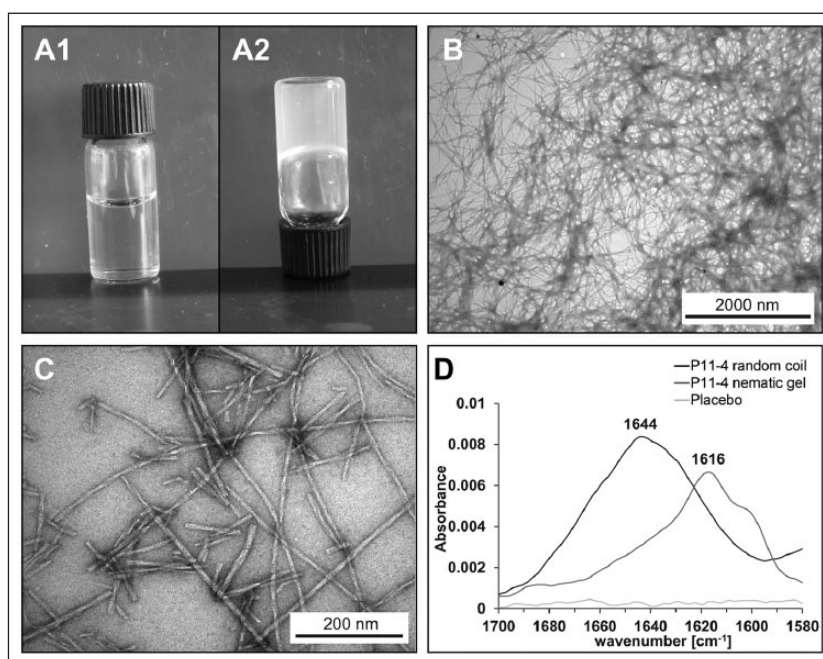mens were then incubated for 1 h in 0.14 M Congo red solution (in 0.15 M NaCl and 5 mM KH_2PO_4, adjusted to pH 7.4 with NaOH) (Klunk et al. 1989) and washed in remineralization buffer. Analysis was performed with a light microscope (Olympus SZX12, camera: UC30).

Matrix-Assisted Laser Desorption/Ionization with Time-of-Flight Analysis

Enamel specimens treated with P_{11}-4 were drilled out with a hand driller on a cavity-glass plate filled with 200 µL distilled water. The drill dust was collected by addition of 200 µL distilled water, and the samples were purified with Cleanup C18 Pipette Tips (Agilent Technologies). The pipette tips were rinsed 2 × 10 µL with 50 wt% acetonitrile in H_2O and rinsed
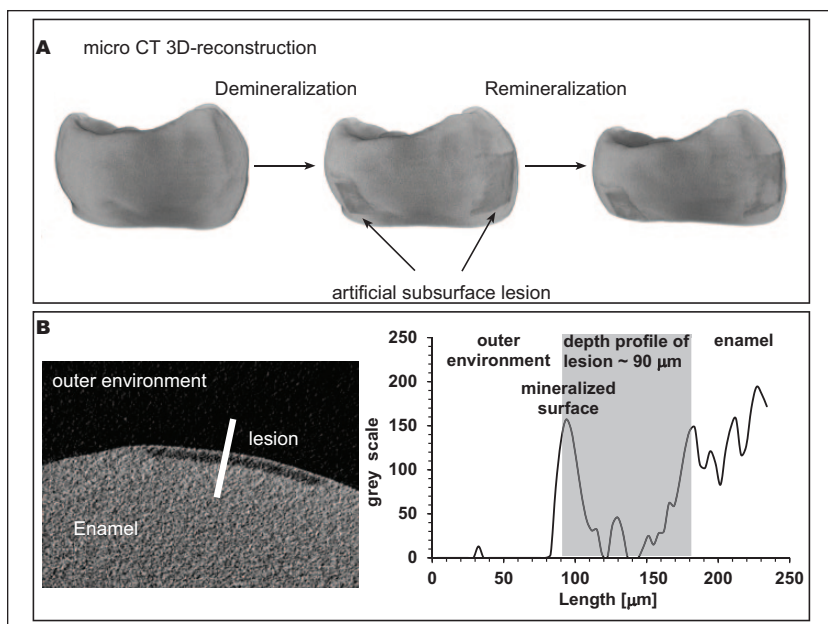
Figure 2. Characterization of artificial carious lesions by micro–computed tomography (μCT). (**A**) Native human tooth (crown only) as reconstructed μCT image. After demineralization, 2 defined windows of demineralization are visible on the surface, becoming less pronounced after remineralization. (**B**) Sample image of a μCT slice showing a demineralized lesion. The artificial lesion is visible as a dark gray band within the enamel and is indicated as such. The graph shows the gray scale along the line indicated in the μCT slice. The mineralized surface layer is clearly visible.

at the ratio of 1:20 and applied on the lesion. Samples were placed in an ibidi-slide in dest. water and analyzed by a confocal laser microscope (Olympus IX81). The recorded stack of four 2-dimensional images each projected the lesion volume of 51.4 μm thickness, giving a total assessment depth of 205 μm (objective: UPLSAPO 20×/NA 0.75; helium-neon gas laser; excitation: 633 nm and emission: 668 nm). Images were analyzed by Olympus software (FluoView FV1000).

Micro–Computed Tomography

Scans were performed before and after incubation on SkyScan1172 high-resolution micro–computed tomography (μCT) (85 kV and 118 μA; Cu/Al filter [0.5 mm]; exposure: 1470 ms; 360° rotation; voxel dimension: 5 μm). Reconstructions (ring-artifact correction: 10; beam-hardening correction: 86%) were done with NRecon (SkyScan, version 1.6.9.8) and image analysis with CTAn (SkyScan, version 1.13.11.0) and CTVol (SkyScan, version 2.23.0). The lesion volume of the demineralized data set was extracted as a binary mask, which was subsequently applied to the followed reference and sample data set. As a consequence, the remineralization degree can be indicated as a ratio between the number of voxels from the final volume and the binary mask.

$2\times$ with 10 μL 0.1 M triethylammonium acetate in $H_2O + 1\%$ 1 M NH_4OH, and then the sample was pipetted 10×10 μL and washed with $3 \times 0.1\%$ trifluoroacidic acid (TFA) in H_2O. Finally, the sample was eluted with 10 μL 50% acetonitrile in H_2O. Then, 1.5 μL of the matrix (20 mg/mL 3,5-dimethoxy-4-hydroxycinnamonacid in H_2O/acetonitrile [1:1] + 0.1% TFA) and 1.5 μL of the sample solution were applied on the sample holder (MTP384 polished steel plate; Bruker), and 2 μL of the calibration standard (protein calibration standard, mass range: ~1,000–3,500 Da; Bruker) was pipetted onto a separate spot. Mass spectra were acquired over a mass/charge (m/z) ratio of 520 to 3,200 using Ultraflex TOF/TOF (Bruker). The mass spectrometer is equipped with a nitrogen (N_2) laser and operates at a wavelength of 337 nm with laser power of 22% (50 laser shots over 5 sides on each sample). Measurements and analysis were performed with FlexControl (Bruker, version 2.4) and FlexAnalysis (Bruker, version 2.4).

Radioactive and Fluorescence Experiments

For radioactive experiments, ^{14}C-P_{11}-4 (6.3 mM) was mixed with P_{11}-4 (6.3 mM) (Table) to obtain an overall radioactivity of 10,000 Bq and applied to enamel specimens following acidification and direct placement in remineralization buffer for 14 d. The peptide in the remineralization solution (i.e., not attached to the enamel specimen) was detected by the scintillation counter (Tri-Cab B2910TR; PerkinElmer).

The fluorescence-labeled peptide samples were prepared by mixing ATTO 647-P_{11}-4 (6.3 mM) and P_{11}-4 (6.3 mM) (Table)

Results

Verification of P_{11}-4 Self-Assembling Structure

In acidic conditions, self-assembled peptide P_{11}-4 forms a nematic gel (Aggeli, Bell, Carrick, et al. 2003), shown in the inverted glass vial (Fig. 1A). This superordinate 3-dimensional network originates in fiber junctions, visible in transmission electron microscopy (TEM) (Fig. 1B, C). FTIR spectra between 1,400 and 1,800 cm^{-1} show a defined absorption band at 1,644 cm^{-1} present in the spectra of the monomeric P_{11}-4 (pD ~8), whereas the fibrillary form of P_{11}-4 (pD <2) shows an absorption band at 1,616 cm^{-1} (Fig. 1D). Reference placebo sample exhibited no absorption in the area of interest.

Creating Artificial Carious Lesions in Human Enamel Specimens

Artificial subsurface carious lesions were created in human specimens. Characterization of the lesions was carried out by light microscopy (LM) and μCT (Fig. 2A). The subsurface lesions with an area of 4 × 4 mm were visible after 3 d in demineralization buffer and showed a lesion depth of 70 ± 23 μm as determined by μCT (Fig. 2B).

Detection of P$_{11}$-4 within an Artificial Caries Lesion

Qualitative Detection of P$_{11}$-4: MALDI-TOF. Matrix-assisted laser desorption/ionization with time-of-flight analysis (MALDI-TOF) spectra of a P$_{11}$-4 solution show a peak at 1,596 m/z (Fig. 3A1). Baseline spectra of ground enamel show no peaks above 1,100 m/z (data not shown). Ground enamel originating from the artificial lesion body treated with P$_{11}$-4 displays the corresponding peptide mass peak at 1,596 m/z (Fig. 3A2). After 14 d, remineralization the mass peak of 1,596 m/z is still clearly visible (Fig. 3A3).

Depth of Penetration into Artificial Lesions of P$_{11}$-4: Confocal Microscopy. Lesions visualized in confocal microscopy with placebo and unlabeled P$_{11}$-4 showed no fluorescence signal (data not shown). The artificial lesions treated with fluorescence-tagged ATTO647-P$_{11}$-4 (Fig. 3B1–2) displayed significant fluorescence signal up to the third 2-dimensional projection covering the depth of the enamel specimen from 103 to 154 μm. After remineralization, fluorescence signal was detected up to the second 2-dimensional projection covering the depth of the enamel specimen from 52 to 103 μm (Fig. 3B3).

P$_{11}$-4 Self-Assembling within Artificial Lesions: Congo Red Staining. Untreated or placebo-treated artificial lesions yielded negative staining with Congo red. Artificial lesions treated with P$_{11}$-4 showed positive staining (Fig. 3C1–3).

Diffusion Behavior of Applied P$_{11}$-4: Radioactive Assay. The scintillation measurements of the daily changed remineralization buffer predicted the amount of P$_{11}$-4 remaining within the lesion. At the first measurement after 1 h (0.04 d), 36% ± 8% of the originally applied radioactive-labeled peptide was detected in the buffer. Within 3 d, an additional 33% ± 6% of the radioactive-labeled P$_{11}$-4 was detected in the buffer, leaving 31% ± 11% of the peptide within the enamel specimen. No more radioactivity was detected in the buffer until the end of the measurements at day 14.

Examination of Remineralization Process Facilitated by P$_{11}$-4 in Artificial Caries Lesions by μCT

μCT images were analyzed and represented (Fig. 4). After 14 d of remineralization, the placebo-treated specimen showed little
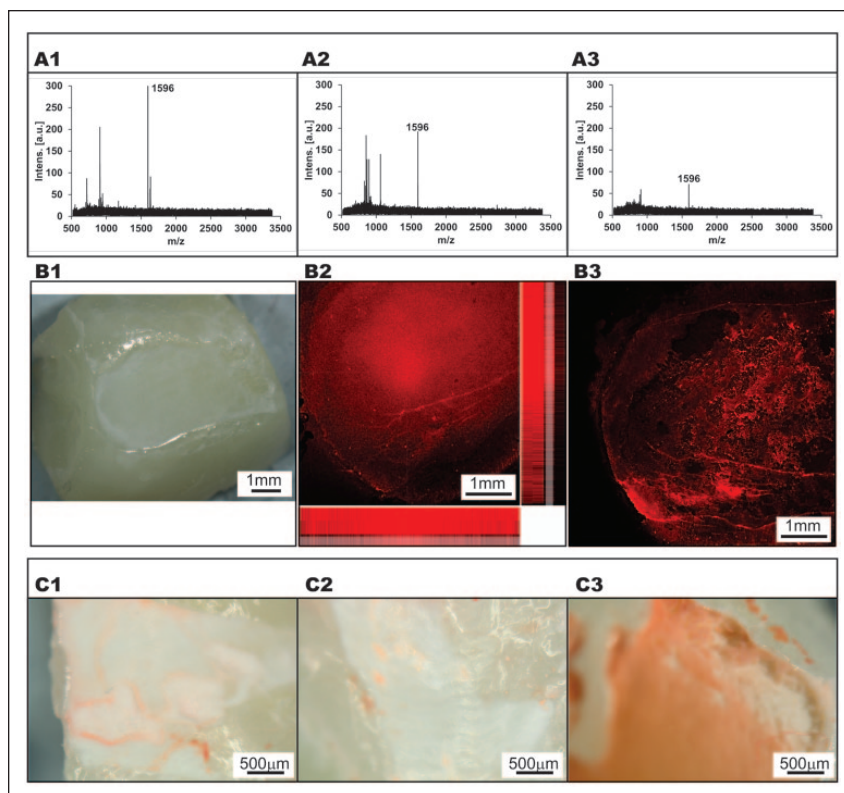

Figure 3. P$_{11}$-4 characterization within an artificial carious lesion. (**A**) Matrix-assisted laser desorption/ionization with time-of-flight analysis mass spectra of (A1) pure monomeric P$_{11}$-4 (A2) ground enamel originating from the artificial lesion body treated with P$_{11}$-4 (self-assembled). (A3) Ground enamel originating from the artificial lesion body treated with P$_{11}$-4 left in remineralization buffer for 14 d. (**B**) Confocal microscopy picture of artificial enamel lesions treated with fluorescence-labeled P$_{11}$-4 (ATTO647-P11-4). (B1) Light microscopy image of artificial carious lesion at baseline prior to application of fluorescence-labeled peptide. (B2) Lesion treated with fluorescence-labeled ATTO647-P$_{11}$-4 after treatment (20× magnification). The side bars show fluorescence with respect to the depth of the lesion; each of the lines corresponds to a 52-μm depth. (B3) After 14 d in remineralization buffer (20× magnification). (**C**) Congo red staining of artificial subsurface carious lesions: (C1) untreated and (C2) placebo-treated lesions show no staining with Congo red. (C3) P$_{11}$-4 treated lesions showing marked staining with Congo red.

remineralization (Fig. 4D1–2, 4E1–2). Specimens treated with P$_{11}$-4 solution showed significant remineralization (Fig. 4F1–2, 4G1–2).

Discussion

The present research supports the forward-looking objective to manage caries lesions noninvasively by biomimetic remineralization (Cochrane et al. 2010). As previously described, the peptide P$_{11}$-4 assembles into a 3-dimensional network under physiological conditions present within carious lesions and is capable of triggering nucleation of de novo hydroxyapatite crystals (Kirkham et al. 2007).

To ensure that the selected formulations of P$_{11}$-4 solutions for the performed experiments were suitable, TEM analysis and FTIR were used to observe the self-assembling fiber matrix formation. Generally, the physicochemical properties of self-assembling peptide P$_{11}$-4 are in agreement with previously
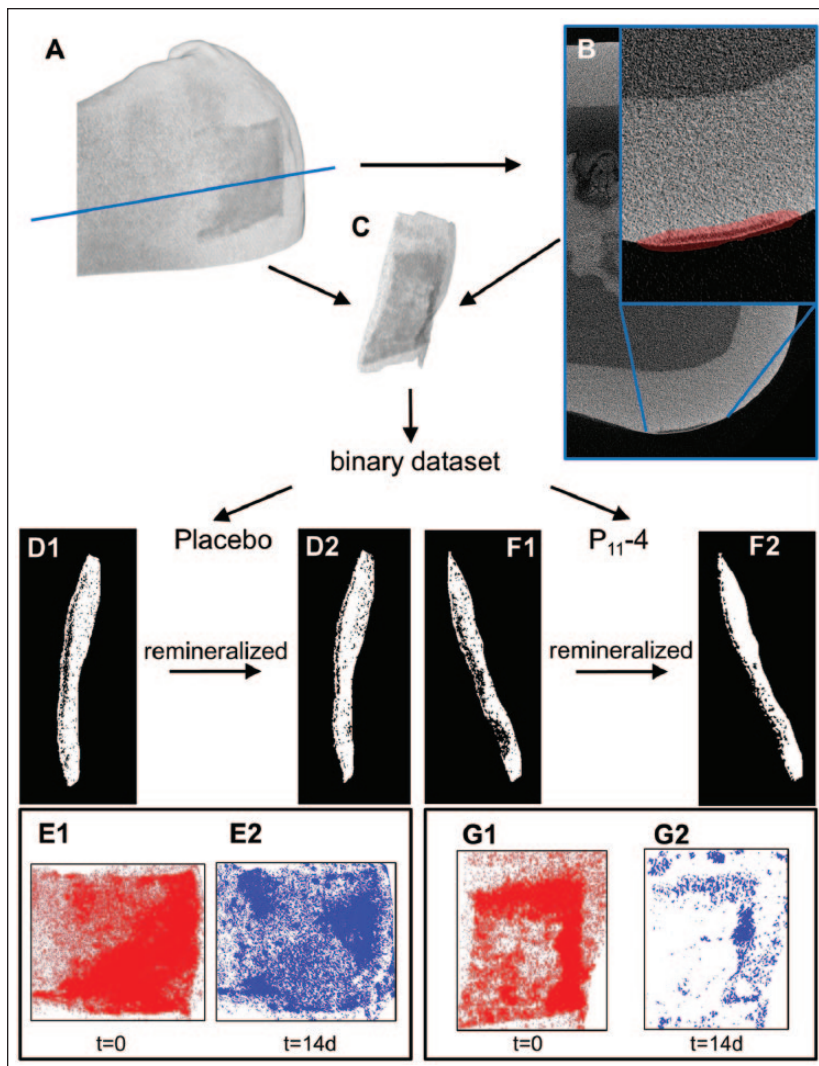
Figure 4. Projections of the micro–computed tomography images before and after remineralization of untreated and P_{11}-4 treated enamel specimens: (**A**) 3-dimensional projection of demineralized tooth and (**B**) 2-dimensional projection of the tooth slide (blue line). The region-of-interest function was used to separate the demineralized area in all 3 dimensions (insert: red highlighted area). (**C**) Three-dimensional projection of demineralized area separated from sound enamel and air at the outer surface was converted to a binary data set. (**D1**) Binary image from data set and (**E1**) 3-dimensional model of untreated demineralized specimen with white spot lesion at baseline (t = 0); red color indicates areas of demineralization. (**D2**) Binary image from data set and (**E2**) 3-dimensional model of corresponding specimen treated with placebo and after placement in remineralization solution; blue color indicates areas of still remaining demineralization after 14 d of remineralization. (**F1**) Binary image from data set and (**G1**) 3-dimensional model of untreated demineralized specimen with white spot lesion at baseline (t = 0). (**F2**) Binary image from data set and (**G2**) 3-dimensional model of corresponding specimen after treatment with P_{11}-4 and after placement in remineralization solution (t = 14 d).

published results (Aggeli, Bell, Boden, et al. 2003; Carrick et al. 2007).

The available ex vivo model of artificial caries lesions in human enamel specimens provided a near-physiological basis for the mechanistic studies of P_{11}-4 in the remineralization of carious lesions. The artificial carious lesions formed within 3 d were comparable to those described in Lo et al. (2010). Depending on the tooth specimen, the depth (70 ± 23 μm) and

the demineralization of the induced lesion were different among teeth, showing the natural variation of enamel.

Main objective of this work was to verify the mechanism of action of the self-assembled peptide. Mass spectrometry has shown that P_{11}-4 diffused into artificial carious lesions, and detectable amounts remained within the lesion body during remineralization. MALDI-TOF data provided qualitative information on the presence of P_{11}-4. Due to mass spectrometry sample preparation in basic pH, the peptide was detected in a monomeric state at 1,596 m/z.

The penetration depth of P_{11}-4 into the subsurface lesions was addressed by confocal microscopy using a mixture of P_{11}-4 and fluorescent-labeled fusion peptide ATTO647-P_{11}-4. By incorporating a short spacer between peptide sequence and the fluorescent marker, the self-assembling ability with unlabeled P_{11}-4 (ratio: 1:20) was given (data not shown) (Fig. 3B1–3). The detected fluorescence signal showed diffusion of P_{11}-4 throughout and beyond the borders of the artificial lesion as defined by μCT. Presumably, this area outside the visible white spot became porous during the demineralization procedure and thus enabled diffusion of monomeric fluorescence-labeled P_{11}-4. After remineralization, the fluorescence signal of presumably fully assembled P_{11}-4 was detected throughout the whole artificial lesion.

Self-assembled fibers of P_{11}-4 could be detected by Congo red staining. It is believed that Congo red binding depends on the secondary conformation of the fibril, consisting predominantly of cross β-pleated sheets. The structure of Congo red suggests that binding could occur through a combination of hydrophobic interactions of benzidine centers, and electrostatic charged terminal groups (Klunk et al. 1989; Frid et al. 2007). Aggeli, Nyrkova, et al. (2001) have shown that P_{11}-4 assembles via antiparallel β-sheets. This is in agreement with negative staining for monomeric peptides and positive staining for P_{11}-4 fibers.

Radioactive-labeled P_{11}-4 was used to quantify the amount of P_{11}-4 originally attached to the enamel specimen and ultimately remaining within the lesion body over time by determining the radioactivity of ^{14}C-P_{11}-4 detected in the remineralization buffer. After 1 h, 36% of the applied P_{11}-4 was detected in the buffer, suggesting that this amount never or only very weakly bound to the enamel specimens, as there was no washing step between the application and the immersion into the buffer.

Throughout the following 3 d, an additional 33% of the originally applied peptide was detected in the buffer, indicating that this amount bound weakly to the mineralized surface and might have been detached due to competitive binding with ions from the remineralization buffer or diffused back out of the lesion as a monomer or small aggregate. The remaining 31% of the applied peptide stayed with the enamel specimen throughout the course of the 14-d detection, as no more radioactivity was recorded in the buffer thereafter. This suggests that 31% of the applied P_{11}-4 formed the scaffold within the lesion. Intriguingly, the concentration of P_{11}-4 within the 1-mm^3 lesion was approximately 2.5× higher than the originally applied peptide concentration (25 mg/mL vs. 10 mg/mL), implying that the self-assembly of the peptide is similar to a precipitation reaction removing the monomers from the solution and driving the diffusion reaction of the peptide into the lesion.

The authors are fully aware that the amount of the peptide self-assembling into fibers and remaining inside the lesion may vary among natural lesions, which differ in size, depth, and shape from the artificial lesions used in this study. Nevertheless, it is worthwhile to further investigate whether the application of P_{11}-4 monomers onto a carious lesion causes a higher concentration of P_{11}-4 within the lesion and what consequences this might have on the importance of original peptide concentration of monomeric P_{11}-4 applied in the treatment.

Nondestructive μCT imaging was chosen to monitor remineralization within the artificial carious lesion. As calculated from and visualized by μCT imaging (Fig. 4), specimens remineralized in the presence of P_{11}-4 had an increase in mineralization of 68% within 14 d, in agreement with previously published data (Davies et al. 2015; Deyhle et al. 2015). In contrast, the spontaneous remineralization of the placebo reference showed a mineral gain of 20%, strongly suggesting that P_{11}-4 enabled a significantly higher degree of remineralization.

The qualitative techniques used in this study established the mechanism of action but were not suitable to characterize the structural arrangement of the mineral within the carious lesion. Earlier in vitro data have indicated that the de novo hydroxyapatite crystals formed around P_{11}-4 fibers are tangentially arranged, forming a fan-type structure. As previous attempts to create prismatic enamel in vitro were futile, the observed mineralization triggered by P_{11}-4 fibers within the subsurface lesion may present a significant step toward regeneration of enamel.

Conclusion

The presented experiments support the proposed mechanism of action for self-assembling peptide P_{11}-4 in regeneration of enamel tissue. Furthermore, it could be shown that P_{11}-4 fibers form throughout the lesion body, potentially enabling regeneration of deeper subsurface lesions.

Author Contributions

L. Kind, contributed to conception, design, and data acquisition, drafted and critically revised the manuscript; S. Stevanovic, S. Wuttig, S. Wimberger, J. Hofer, contributed to data acquisition, analysis, and interpretation, critically revised the manuscript; B. Müller, contributed to conception, critically revised the manuscript; U. Pieles, contributed to conception and design, critically revised the manuscript. All authors gave final approval and agree to be accountable for all aspects of the work.

References

Aggeli A, Bell M, Boden N, Carrick LM, Strong AE. 2003. Self-assembling peptide polyelectrolyte beta-sheet complexes form nematic hydrogels. Angew Chem Int Ed Engl. 42(45):5603–5606.

Aggeli A, Bell M, Boden N, Keen JN, Knowles PF, McLeish TC, Pitkeathly M, Radford SE. 1997. Responsive gels formed by the spontaneous self-assembly of peptides into polymeric beta-sheet tapes. Nature. 386(6622):259–262.

Aggeli A, Bell M, Carrick LM, Fishwick CW, Harding R, Mawer PJ, Radford SE, Strong AE, Boden N. 2003. Ph as a trigger of peptide beta-sheet self-assembly and reversible switching between nematic and isotropic phases. J Am Chem Soc. 125(32):9619–9628.

Aggeli A, Fytas G, Vlassopoulos D, McLeish TC, Mawer PJ, Boden N. 2001. Structure and dynamics of self-assembling beta-sheet peptide tapes by dynamic light scattering. Biomacromolecules. 2(2):378–388.

Aggeli A, Nyrkova IA, Bell M, Harding R, Carrick L, McLeish TC, Semenov AN, Boden N. 2001. Hierarchical self-assembly of chiral rod-like molecules as a model for peptide beta-sheet tapes, ribbons, fibrils, and fibers. Proc Natl Acad Sci U S A. 98(21):11857–11862.

Bertassoni LE, Habelitz S, Marshall SJ, Marshall GW. 2011. Mechanical recovery of dentin following remineralization in vitro—an indentation study. J Biomech. 44(1):176–181.

Bröchner A, Christensen C, Kristensen B, Tranaeus S, Karlsson L, Sonnesen L, Twetman S. 2010. Treatment of post-orthodontic white spot lesions with casein phosphopeptide-stabilised amorphous calcium phosphate. Clin Oral Investig. 15(3):369–373.

Brookes SJ, Kirkham J, Shore RC, Wood SR, Slaby I, Robinson C. 2001. Amelin extracellular processing and aggregation during rat incisor amelogenesis. Arch Oral Biol. 46(3):201–208.

Brunton PA, Davies RP, Burke JL, Smith A, Aggeli A, Brookes SJ, Kirkham J. 2013. Treatment of early caries lesions using biomimetic self-assembling peptides—a clinical safety trial. Br Dent J. 215(4):E6.

Carneiro KM, Zhai H, Zhu L, Horst JA, Sitlin M, Nguyen M, Wagner M, Simpliciano C, Milder M, Chen CL, et al. 2016. Amyloid-like ribbons of amelogenins in enamel mineralization. Sci Rep. 6:23105.

Carrick LM, Aggeli A, Boden N, Fisher J, Ingham E, Waigh TA. 2007. Effect of ionic strength on the self-assembly, morphology and gelation of pH responsive β-sheet tape-forming peptides. Tetrahedron. 63(31):7457–7467.

Cochrane NJ, Cai F, Huq NL, Burrow MF, Reynolds EC. 2010. New approaches to enhanced remineralization of tooth enamel. J Dent Res. 89(11):1187–1197.

Davies RP, Aggeli A, Boden N, McLeish TC, Nyrkova IA, Semenov AN. 2009. Mechanisms and principles of 1D self-assembly of peptides into [beta]-sheet tapes. In: Rudy JK, editor. Advances in chemical engineering. New York: Academic Press. p. 11–43.

Davies RP, Howard R, Thomson BM, Brookes SJ, Lysek DA, Kirkham J. 2015. Treatment of fabricated caries lesions: self-assembling peptides vs. fluoride. Caries Res. 49(2015):359.

Deyhle H, Dziadowiec I, Kind L, Thalmann P, Schulz G, Müller B. 2015. Mineralization of early stage carious lesions in vitro—a quantitative approach. Dent J. 3(4):111–122.

Firth A, Aggeli A, Burke JL, Yang X, Kirkham J. 2006. Biomimetic self-assembling peptides as injectable scaffolds for hard tissue engineering. Nanomedicine (Lond). 1(2):189–199.

Frid P, Anisimov SV, Popovic N. 2007. Congo red and protein aggregation in neurodegenerative diseases. Brain Res Rev. 53(1):135–160.

Goldberg M, Septier D, Lecolle S, Chardin H, Quintana MA, Acevedo AC, Gafni G, Dillouya D, Vermelin L, Thonemann B, et al. 1995. Dental mineralization. Int J Dev Biol. 39(1):93–110.

Hannig M, Hannig C. 2010. Nanomaterials in preventive dentistry. Nat Nanotechnol. 5(8):565–569.

Hara AT, Zero DT. 2010. The caries environment: saliva, pellicle, diet, and hard tissue ultrastructure. Dent Clin North Am. 54(3):455–467.

Jablonski-Momeni A, Heinzel-Gutenbrunner M. 2014. Efficacy of the self-assembling peptide p11-4 in constructing a remineralization scaffold on artificially-induced enamel lesions on smooth surfaces. J Orofac Orthop. 75(3):175–190.

Kassebaum NJ, Bernabe E, Dahiya M, Bhandari B, Murray CJ, Marcenes W. 2015. Global burden of untreated caries: a systematic review and metaregression. J Dent Res. 94(5):650–658.

Kayser V, Turton DA, Aggeli A, Beevers A, Reid GD, Beddard GS. 2004. Energy migration in novel pH-triggered self-assembled beta-sheet ribbons. J Am Chem Soc. 126(1):336–343.

Kirkham J, Brookes SJ, Shore RC, Wood SR, Smith DA, Zhang J, Chen H, Robinson C. 2002. Physico-chemical properties of crystal surfaces in matrix–mineral interactions during mammalian biomineralisation. Curr Opin Colloid Int Sci. 7(1–2):124–132.

Kirkham J, Firth A, Vernals D, Boden N, Robinson C, Shore RC, Brookes SJ, Aggeli A. 2007. Self-assembling peptide scaffolds promote enamel remineralization. J Dent Res. 86(5):426–430.

Kirkham J, Zhang J, Brookes SJ, Shore RC, Wood SR, Smith DA, Wallwork ML, Ryu OH, Robinson C. 2000. Evidence for charge domains on developing enamel crystal surfaces. J Dent Res. 79(12):1943–1947.

Klunk WE, Pettegrew JW, Abraham DJ. 1989. Quantitative evaluation of Congo red binding to amyloid-like proteins with a beta-pleated sheet conformation. J Histochem Cytochem. 37(8):1273–1281.

Li R, Guo W, Yang B, Guo L, Sheng L, Chen G, Li Y, Zou Q, Xie D, An X, et al. 2011. Human treated dentin matrix as a natural scaffold for complete human dentin tissue regeneration. Biomaterials. 32(20):4525–4538.

Lo EC, Zhi QH, Itthagarun A. 2010. Comparing two quantitative methods for studying remineralization of artificial caries. J Dent. 38(4):352–359.

Maude S, Ingham E, Aggeli A. 2013. Biomimetic self-assembling peptides as scaffolds for soft tissue engineering. Nanomedicine (Lond). 8(5):823–847.

Nyrkova IA, Semenov AN, Aggeli A, Bell M, Boden N, McLeish TC. 2000. Self-assembly and structure transformations in living polymers forming fibrils. Eur Phys J B. 17(3):499–513.

Petersen PE. 2003. The world oral health report 2003: continuous improvement of oral health in the 21st century—the approach of the WHO global oral health programme. Community Dent Oral Epidemiol. 31(Suppl 1):3–23.

Ruan Q, Moradian-Oldak J. 2015. Amelogenin and enamel biomimetics. J Mater Chem B Mater Biol Med. 3:3112–3129.

Schlee M, Rathe F, Schad T, Koch JH, Tjaden A, Bommer C. 2014. Klinischer effekt biomimetischer mineralisation bei approximalkaries. Stomatologie 111(4–5):175–181.

Schmidlin P, Zobrist K, Attin T, Wegehaupt F. 2016. In vitro re-hardening of artificial enamel caries lesions using enamel matrix proteins or self-assembling peptides. J Appl Oral Sci. 24(1):31–36.

Semino CE. 2008. Self-assembling peptides: from bio-inspired materials to bone regeneration. J Dent Res. 87(7):606–616.

Takahashi F, Kurokawa H, Shibasaki S, Kawamoto R, Murayama R, Miyazaki M. 2016. Ultrasonic assessment of the effects of self-assembling peptide scaffolds on preventing enamel demineralization. Acta Odontol Scand. 74(2):142–147.

ten Cate JM. 1997. Review on fluoride, with special emphasis on calcium fluoride mechanisms in caries prevention. Eur J Oral Sci. 105(5 Pt 2):461–465.

ten Cate JM, Arends J. 1980. Remineralization of artificial enamel lesions in vitro: III. A study of the deposition mechanism. Caries Res. 14(6):351–358.

Thomson BM, Hardaker L, Davies RP, Dennis C, Bronowska A, Aggeli A, Kirkham J, Lysek DA. 2014. P11-15 (nnrfewefenn): a biocompatible, self-assembling peptide with potential to promote enamel remineralisation. Paper presented at: 61 ORCA Congress; Greifswald, Germany.